European Journal of Pharmaceutics and Biopharmaceutics 76 (2010) 127–137

Contents lists available at ScienceDirect

European Journal of Pharmaceutics and Biopharmaceutics

journal homepage: www.elsevier.com/locate/ejpb

Research paper

Non-destructive methods of characterization of risperidone solid lipid nanoparticles

Ziyaur Rahman, Ahmed S. Zidan, Mansoor A. Khan *

Division of Product Quality and Research, Center of Drug Evaluation and Research, Food and Drug Administration, Silver Springs, MD, USA

ARTICLE INFO

Article history:
Received 25 February 2010
Accepted in revised form 7 May 2010
Available online 12 May 2010

Keywords:
Risperidone
Compritol 888 ATO
SLN
NIR
NIR-CI

ABSTRACT

The objective of this investigation is to evaluate compositional variations and their interaction of the solid lipid nanoparticle (SLN) formulation of risperidone using response surface methodology of design of experiment (DOE) and subsequently, characterize the SLN by non-destructive methods of analysis. Box–Behnken DOE was constructed using drug (X_1), lipid (X_2) and surfactant (X_3) level as independent factors. Compritol 888 ATO and sodium lauryl sulphate were used as lipid and surfactant, respectively. The SLN was prepared by solvent evaporation method and characterized by transmission electron microscopy (TEM), differential scanning calorimetry (DSC), X-ray powder diffraction (XRD), fourier infrared spectroscopy (FTIR), near infrared spectroscopy (NIR) and NIR-chemical imaging (NIR-CI). Responses measured were entrapment efficiency (Y_1), D_{90} (Y_2), zeta potential (Y_3), burst effect (Y_4) and cumulative release in 8 h (Y_5). Statistically significant ($p < 0.05$) effect of X_1 on the Y_1, Y_2, Y_3 and Y_4 were seen. FTIR revealed no interaction between risperidone and compritol 888 ATO. TEM showed spherical and smooth surface SLN. Compritol retained its crystalline nature in the SLN formulation revealed by DSC and XRD studies. Homogenous distribution of risperidone and compritol 888 ATO was revealed by NIR-CI. Principal component analysis (PCA) and partial least square (PLS) were carried out on NIR data of SLN formulation. PLS showed correlation coefficient > 0.996 for prediction and calibration model of both risperidone and compritol 888 ATO. The accuracy of models in predicting risperidone and compritol 888 ATO were 1.60% and 11.27%, respectively. In conclusion, the DOE reveals significant effect of drug loading on SLN characteristics, and chemometric models based on NIR and NIR-CI data provided non-destructive method of estimation of components of SLN.

Published by Elsevier B.V.

1. Introduction

Delivering therapeutic agents directly to the diseased organ or tissue has been a challenge for formulation scientist. It is expected that a good delivery strategy to a disease organ will improve the therapeutic index of a drug and reduce the side effects associated with it. One such organ is brain, and physicians have an acute need to deliver drugs directly to the brain to treat the conditions such as Parkinsonism, Alzheimer, stroke and gliomas. The traditional methods with conventional dosage forms are ineffective or associated with severe side effects of a drug. Over the decades, many strategies have been devised to enhance delivery of drug to brain in order to improve therapeutic index of a drug. Both invasive and non-invasive techniques have been reported. Invasive methods include intraventricular [1] or intracerebral [2] infusion and intracerebral implant for controlled drug release [3]. Non-invasive techniques are prodrugs [4], conjugation with antibodies [5], alternate route of administration (intranasal administration) [6] and colloidal drug delivery systems. Among the reported strategies, colloidal delivery system seems to be gaining momentum because of their ability to deliver drugs successfully to brain without altering the blood brain barrier property. Colloidal delivery systems reported for brain delivery systems are polymeric micelles [7], liposomes [8], polymeric nanoparticles [9] and solid lipid nanoparticles [10]. The SLN combines the advantages of polymeric nanoparticles, liposomes, fat emulsion while avoiding their disadvantages [10]. Some advantages offered by SLN are stability of even up to three years [11], high drug payload, scalability, sterilizability [12,13] and feasibility of delivering both lipophilic and hydrophilic drugs. The carrier lipids are mostly GRAS (generally regarded as safe). The reasons for efficient delivery of drug SLN are due to enhanced retention in brain–blood capillaries resulting in an enhanced concentration gradient across the blood brain barrier that leads to opening of tight junction and transcytosis [10].

Traditional pharmaceutical development involves trial and error method for the process and formulation optimization. Pharmaceutical development is the process of design of quality product and understanding the process that consistently deliver the

* Corresponding author. Address: FDA/CDER/DPQR, White Oak, LS Building 64, Room 1070, 10903 New Hampshire Ave., Silver Spring, MD 20993-002, USA. Tel.: +1 301 796 0016; fax: +1 301 796 9816.
E-mail address: Mansoor.Khan@fda.hhs.gov (M.A. Khan).

0939-6411/$ - see front matter Published by Elsevier B.V.
doi:10.1016/j.ejpb.2010.05.003

product for intended performance. The knowledge gained during pharmaceutical development will help to define the design space for a formulation and/or a process. Design space is a multidimensional combination and interaction of input variables (e.g., material attributes) and process parameters that have been demonstrated to provide assurance of quality [14]. It is expected that critical quality attributes (CQA) of a product are maintained as long as changes made in process parameters, and formulation attributes are within the defined design space. Design of experiment (DOE) is the methodology of systemically determining the relationship between variables affecting the formulation and/or process and output of that formulation and/or process [14]. It is the statistical way of testing large number of formulation and process variables in a minimum number of experiment run. Response surface method is commonly used to estimate main effect, their interaction, quadratic effects and shape of response surface. The central composite design and Box–Behnken are the most commonly used design for response surface methodology [15]. The Box–Behnken design has advantage over central composite in that it requires fewer run when the numbers of factors investigated are three. It loses this advantage when number of factor investigated goes to four [16]. It is an independent quadratic design in that it does not contain embedded factorial or fractional factorial design. In this design factor, combination is at the midpoint of edges of the process space and at the center. These designs are rotatable and require three levels of each factor [15].

The purpose of this research is to evaluate main and interaction effect of compositional variation and optimization of a solid lipid nanoparticle formulation of risperidone by design of experiment approach. Secondly, to estimate the components of SLN formulations by non-destructive methods such as near infrared spectroscopy (NIR) and NIR-chemical imaging using PLS method of chemometrics for a better control strategy. Risperidone was selected as a model compound to prepare SLN because it is a second generation antipsychotic agent used to control and treat schizophrenia [17]. It was reported to be the only drug approved by FDA for the treatment of schizophrenia in 13–17 years age group of children and bipolar mania [18].

2. Materials and methods

2.1. Materials

Risperidone was obtained from Erregierre S.p.A, San Paolo D'Argon, BG. Compritol 888 ATO was obtained by Gattefosse Corporation, Paramus, NJ, USA. Sodium lauryl sulphate, methanol, acetone, chloroform were obtained from Fisher Scientific Co., Norcross, GA, USA. All other reagents and solvents used were of analytical grade or better.

2.2. Methods

2.2.1. Design of experiment

Box–Behnken quadratic response surface design was constructed to optimize the solid lipid nanoparticle formulation with 15 experiments with points laying at on the middle of each edge of multidimensional cube and center point replicate ($n = 3$) was designed using software JMP version 7.0.1 (SAS, NC, USA). This model is described by following quadratic equation:

$$Y = b_0 + b_1X_1 + b_2X_2 + b_3X_3 + b_{12}X_1X_2 + b_{23}X_2X_3 + b_{13}X_1X_3 + b_{11}X_1^2 + b_{22}X_2^2 + b_{33}X_3^2$$

where Y is the measured response associated with each factor level combinations; b_0 is the intercept and b_1 to b_{33} are the regression coefficient computed from observed value of Y; X_1, X_2 and X_3 are coded level of independent variables. The X_iX_j ($i = 1$, 2 or 3 and $j = 1$, 2 or 3) and $X_i^2 (i = 1, 2 \text{ or } 3)$ are interaction and quadratic terms, respectively.

The independent factors selected were risperidone (X_1), compritol (X_2) and sodium lauryl sulphate (X_3) and their low, medium and high levels are shown in Table 1. The dependent responses studied were entrapment efficiency (Y_1), particles size (Y_2), zeta potential (Y_3), burst release (Y_4) and drug release (Y_5). The experiment design matrix is shown in Table 2.

2.2.2. Solid lipid nanoparticle preparation

Solid lipid nanoparticles were prepared by emulsion-solvent evaporation method [19]. Briefly, required amount of risperidone and compritol 888 ATO were dissolved in 20 ml of chloroform. It was added into 200 ml of sodium lauryl sulphate aqueous solution while homogenizing at 6000 rpm by probe type homogenizer PowerGen 125 (Fisher Scientific, PA, USA) for 10 min and at the same time, stirred by mechanical mixer at 300 rpm to prevent any dead zone of unhomogenized area in the mixing beaker. After that, it was stirred mechanically at 1000 rpm for 2 h during that period all the solvent will evaporate leaving solid residue of nanoparticle. The nanoparticle was retrieved by centrifugation at 49,500*g* (RC-5C, Sorwall Instruments/Thermo Scientific, MA, USA) for 1 h and washed twice with deionized water to remove surfactant. Before centrifugation, 1 ml sample was withdrawn for size distribution measurements. The retrieved nanoparticles were resuspended in 2 ml of deionized water and frozen at −80 °C and freeze-dried in Dry/Shell Freeze System (Labconco Corp., MI, USA) at −10 °C for 48 h. The obtained freeze-dried products were kept in refrigerator until further analysis.

2.2.3. Entrapment efficiency and drug loading

Approximately 25 mg of SLN was dissolved in 5 ml of chloroform and sonicated for 5 min and centrifuged at 15,000 rpm for 15 min to sediment the any insoluble matter. Supernatant was diluted 10 times with mobile phase before injection into the HPLC column. The concentration was determined from the calibration curve of risperidone, and entrapment efficiency and loading efficiency were calculated by the following formula

$$\text{Entrapment efficiency, EFF} = \frac{a \times 100}{b}$$

where a – weight of drug in the nanoparticles, b – weight of drug used in the formulation

$$\text{Loading efficiency, LEF} = \frac{c \times 100}{d}$$

where c – weight of risperidone in solid lipid nanoparticle, d – weight of solid lipid nanoparticles

2.2.4. HPLC analysis

Risperidone was estimated from solid lipid nanoparticle by modified HPLC method reported by Suther et al. [20]. The instrument is Hewlett Packard (HP) HPLC (Agilent technologies, CA, USA) equipped with quaternary HP 1050 pump, HP 1050 autosampler and 1050 HP UV detector set at a wavelength of 280 nm and column compartment thermostatted at 26 °C. The HPLC stationary phase was composed of a reverse phase Luna C18 (2) 4.6 × 250 mm (5 μm packing) column and a C18, 4.6 × 12.5 mm

Table 1
Experimental factors and their levels.

Factor	Level (−)	Level (0)	Level (+)
Risperidone (mg), X_1	100	200	300
Compritol (mg), X_2	300	400	500
Sodium lauryl sulphate (%w/v), X_3	0.050	0.075	0.100

Table 2
Box–Behnken experimental design.

Formulation	Drug (mg, X_1)	Lipid (mg, X_2)	Surfactant (% w/v, X_3)
1	300	400	0.100
2	100	400	0.100
3	300	400	0.050
4	200	500	0.050
5	100	500	0.075
6	300	500	0.075
7	200	400	0.075
8	200	500	0.100
9	200	300	0.050
10	300	300	0.075
11	100	400	0.050
12	200	400	0.075
13	200	400	0.075
14	100	300	0.075
15	200	300	0.100

(5 μm packing) Luna C18 (2) guard column (Phenomenex Torrance, CA, USA). The mobile phase consisted of phosphate buffer (20 mM) pH 7.0: acetonitrile: methanol (40:45:15) and was pumped isocratically at a flow rate of 1 mL/min. The HPLC method was validated as per ICH guidance of method validation [21].

2.2.5. In-vitro release study

The solid lipid nanoparticles were evaluated for drug release property by horizontal shaker method [19]. The nanoparticles equivalent to 4 mg of risperidone were suspended in 100 ml of phosphate buffer pH 7.4 (0.2 M USP buffer), and this volume is sufficient to maintain the sink condition for risperidone [22]. Various replicates were placed on biological shaker at 37 ± 0.5 °C and 120 rpm. At specified time intervals (0.5, 1, 2, 3, 4, 6 and 8 h), 0.5 ml samples were withdrawn and centrifuged at 14,000 rpm for 15 min, and supernatants were analyzed for percentage of drug released by RP-HPLC method. Experiment was performed in triplicate.

2.2.6. Particle size and zeta potential

Particle size and zeta potential were measured by photon correlation spectroscopy using Zetasizer NanoZS (Malvern Instruments Inc., Westborough, MA, USA). The sample retained before centrifugation of SLN was used for particle size estimation. For zeta potential, freeze-dried SLN formulations were suspended in deionized water. All measurements were done at 25 °C and performed in triplicate.

2.2.7. Differential scanning calorimetry

DSC of compritol 888 ATO, risperidone, SLN and their physical mixture were measured with SDT 2960 Simultaneous DSC/TGA (TA Instruments Co., New Castle, DE, USA). The temperature scanning rate was 10 °C/min and scanned up to 200 °C. This temperature range was covering the melting range of both the component of nanoparticles. The nitrogen gas was flowing at a pressure of 20 psi to provide inert atmosphere during the measurement to prevent oxidation reaction.

2.2.8. Fourier transforms infrared spectroscopy

The FTIR spectra of pure components, physical mixture and nanoparticle formulation were measured by ATR-FTIR (Thermo Nicolet Nexus 670 FTIR, GMI Inc., Ramsey, Minnesota, USA), and OMNIC ESP software (version 5.1) was used to capture and analyze the spectra.

2.2.9. X-ray powder diffraction

Diffraction pattern of risperdone, compritol, SLN and their physical mixture were collected on X-ray diffractometer (MD-10 mini diffractometer, MTI Corporation, Richmond, CA, USA) using Cu K 2α rays (λ = 1.54056 Å) with a voltage of 25 kV and a current of 30 mA, in flat plate $\theta/2\theta$ geometry, over the 2θ ranges 15–75°, with a step width 0.05° and a scan time of 2.0 s per step.

2.2.10. Transmission electron microscopy

Morphology of SLN was studied by transmission electron microscopy (TEM, TEOL JFM 100CX, JEOL Inc., MA, USA). Sample of SLN suspension of about 10 L was placed on 300 mesh copper Holey carbon grid (SPI supplies, West Chester, PA, USA). The sample was stained with 2% w/v phosphotungstic acid after complete air drying and visualized for morphology at 80 kV by TEM.

2.2.11. Near infrared spectroscopy

Near infrared (NIR) spectra for all the solid lipid nanoparticles formulation were collected by Foss NIR spectrometer (Rapid Content TM Analyzer, AP-2020, Model 5000, Foss NIR Systems Co., Laurel, MD) equipped with a diffuse reflectance apparatus over the range 1100–2500 nm. The formulation was filled in the 2 ml of borosilicate glass vials, and spectrum was obtained directly scanning through the base of vials. Sextet measurements were collected for each formulation by rotation of sample. Unscramber v9.2 (CAMO Software Inc., Woodbridge, NJ, USA) software was utilized to process and chemometric analysis of spectral data.

2.2.12. Near infrared chemical imaging spectroscopy

The NIR-CI of solid lipid nanoparticles was collected by SapphireIM NIR Spectral Imaging System (Spectral Dimensions, Inc., Olney, MD). The imaging system equipped with liquid crystal tunable filter (LCTF) coupled with a NIR sensitive focal plane array (FPA) detector. The NIR light reflected (via diffuse reflectance) from the samples to the detector, was passed through a LCTF and was imaged onto the indium–gallium–arsenide focal plane array with 256 × 320 pixels. The LCTF selectively allowed a particular wavelength band to pass, and spectral images were recorded stepwise from 1400 to 2450 nm at 10 nm intervals (105 frames). Dark background was collected with dark cube (acquired using a stainless steel mirror) and light background with high reflectance reference cube (acquired using a Spectralon plate, Labsphere, North Sutton, NH) and software, SapphireGo (Spectral Dimensions, Inc., Olney, MD) automatically subtract dark spectrum form sample cube and then divide with light background spectrum to produce a corrected reflectance data cube (hyperspectral). Hyperspectral images were truncated to 50 × 50 pixels. Each spectroscopic image represented the average of eight accumulations (105 spectral frames/accumulation), with each spectral frame recorded at an integration time of 60 ms. The average sampling time was approximately 3 min. Images were analyzed by ISysIM software (Spectral Dimensions, Inc., Olney, MD), each spectrum in the corrected reflectance (R) data cube was converted to absorbance by calculating the logarithm of the inverse of the reflectance ($\log(1/R)$). Then, each spectrum in the absorbance cube was differentiated with the Savitzky–Golay 2nd derivative filter with a length of 11 points (100 nm) and a polynomial order of 3. Pure risperidone and compritol were used to construct the library. PLS concentration score images were generated using PLS analysis type 2.

3. Results and discussion

3.1. Entrapment efficiency (Y_1)

The entrapment efficiency varies from 25.96 (formulation 15) to 95.19% (formulation 3) for various factor level combinations (Table 3). The independent factors affecting the entrapment efficiency were drug (X_1) and surfactant levels (X_3) ($p < 0.05$, Table 4 and

Fig. 1A) used in the manufacturing of solid lipid nanoparticles. The effect could be explained by following quadratic equation

$$Y_1 = 49.7 + 23.33X_1 + 0.56X_2 - 16.16X_3 - 0.46X_1X_2 - 1.74X_1X_3 + 0.12X_2X_3 + 9.86X_1^2 - 0.66X_2^2 + 0.46X_3^2$$

The positive value of a factor in the regression equation indicates the enhancement of that response and vice versa [23]. The model could predict the observed value better than the mean was with 87.4% confidence and a value of correlation coefficient, R^2, '0.959' indicated good correlation between observed and predicted value of entrapment efficiency (Table 3). Significant effects of independent variables are revealed by ANOVA analysis (Table 5).

The entrapment efficiency (Y_1) could be increased with drug concentration (X_1) in the internal phase as more of the drug would be available for entrapment. The lipid level (X_2) has non-significant effect but positive impact on Y_1 as revealed by positive value in the quadratic equation [24]. This is probably due to increase in the viscosity of medium resulting in faster solidification of nanoparticles. This would further prevent the drug diffusion to external phase of the medium [24].

The surfactant level (X_3) has significant but negative impact on the entrapment efficiency (Y_1). This could be explained by partition phenomenon. High surfactant level in the external phase might increase the partition of drug from internal to external phase of the medium. This increased partition of the drug results in the increased solubilization of drug in the external phase [25].

Interaction terms or quadratic relationship are represented by more than one factor or higher-order terms in the regression equation, respectively. It also suggests non-linearity between factors and responses. A factor can produce a different degree of response when a factor is varied at different levels or more than one factor is varied simultaneously. The interaction and quadratic effects of factors levels have non-significant effects on the entrapment efficiency ($p > 0.05$).

3.2. Particle size distribution (Y_2)

D_{90} of solid nanoparticle ranged from 145.27 (formulation 14) to 293.97 nm (formulation 8) (Table 3) with the selected levels of variables. Following equation can describe the Y_2

$$Y_2 = 232.66 + 17.14X_1 + 23.41X_2 - 10.68X_3 - 31.47X_1X_2 + 21.04X_1X_3 + 43.90X_2X_3 - 14.37X_1^2 + 2.68X_2^2 - 0.29X_3^2$$

The most significant factors affecting the D_{90} are drug (X_1) and lipid levels (X_2) ($p < 0.050$, Tables 4 and 5 Fig. 1B). Good correlation was shown between observed and predicted value as revealed by R^2 of 0.961. The confidence that predicted value is better than mean value is 89%.

The drug and lipid levels have positive influence over D_{90} as reported by other investigators [26]. This was because of increased viscosity of inner phase that affected the shearing capacity of homogenizer and stirrer as well. Emulsifier has negative impact on Y_2. This is probably due to increased diffusion of drug from droplet to external phase resulting in smaller particle size. Moreover, it also stabilized the smaller droplet and prevents the coalescence into bigger droplet [27].

Interaction terms have statistically significant effects on Y_2. X_1 and X_2 interaction had negative impact, while interaction terms X_2 and X_3, and X_1 and X_3 had positive influence (Fig. 2). Quadratic effects have non-significant effects on Y_2.

3.3. Zeta potential (Y_3)

Zeta potential is the measure of overall charges acquired by particles in a particular medium and is considered as one of the benchmark of stability of colloidal system. Particles will repel each other if the systems have high positive or negative value of zeta potential, and system having value ±30 mV is considered stable formulation if dispersed in a liquid as colloidal dispersion [23]. The value of zeta potential varied from −52.40 (formulation 10) to −64.90 mV (formulation 5) (Table 3). Following equation can explain the effect of factors levels on Y_3

$$Y_3 = -56.12 + 3.25X_1 - 1.87X_2 - 1.42X_3 + 1.54X_1X_2 + 0.28X_1X_3 + 0.08X_2X_3 - 0.42X_1^2 - 0.56X_2^2 + 0.30X_3^2$$

The drug and lipid have statistical significant effect on the zeta potential ($p < 0.05$, Tables 4 and 5 and Fig. 1C). This could be correlated with zeta potential of pure components and actual drug loading in solid lipid nanoparticles formulation. Risperidone (8.61 ± 5.97 mV) and compritol 888 ATO (−74.4 ± 10.8 mV) have positive and negative value of zeta potential, respectively. Formulations 10 and 5 have highest and lowest drug loading, respectively, and compritol loading would be reverse in those formulation. Increase in zeta potential would be expected in positive direction with increase in drug loading as positive

Table 3
Observed and predicted value of entrapment efficiency (Y_1), particle size (Y_2), zeta potential (Y_3), burst effect (Y_4) and DE (Y_5).

Formulation	Loading (%)	Observed Y_1	Predicted Y_1	Observed Y_2	Predicted Y_2	Observed Y_3	Predicted Y_3	Observed Y_4	Predicted Y_4	Observed Y_5	Predicted Y_5
1	30.41	70.96	65.47	239.52	245.50	−54.40	−54.58	24.25	24.53	76.42	69.42
2	6.07	28.35	22.27	161.51	169.14	−60.20	−61.66	16.06	14.08	46.53	39.12
3	40.79	95.19	101.27	232.39	224.77	−52.87	−51.41	23.65	25.63	75.69	83.10
4	22.52	72.80	66.10	213.92	225.22	−54.27	−56.02	27.12	24.21	52.62	45.90
5	5.90	35.38	36.58	264.02	258.70	−64.90	−63.33	15.85	19.03	36.94	36.66
6	30.64	81.72	82.34	233.71	230.03	−54.03	−53.73	24.72	25.65	66.93	66.24
7	15.79	47.38	49.70	218.98	232.66	−56.97	−56.12	21.21	22.36	48.62	58.89
8	6.95	29.15	34.03	293.97	291.67	−59.47	−59.59	26.5	25.30	38.48	46.18
9	28.85	70.11	65.24	263.91	266.21	−53.13	−53.01	29.56	30.77	73.76	66.07
10	41.67	83.34	82.14	240.85	246.17	−52.40	−53.98	31.41	28.23	77.43	77.71
11	8.53	45.63	51.12	238.56	232.58	−57.53	−57.35	21.08	20.80	41.25	48.25
12	20.29	51.86	49.70	245.72	232.66	−54.93	−56.12	22.54	22.36	62.85	58.89
13	18.09	49.87	49.70	233.27	232.66	−56.47	−56.12	23.32	22.36	65.21	58.89
14	8.79	35.17	34.55	145.27	148.95	−57.10	−57.40	20.5	19.57	41.45	42.14
15	7.59	25.96	32.66	168.37	157.07	−58.67	−56.92	18.95	21.86	36.24	42.96
R^2			0.959		0.961		0.887		0.811		0.833

Table 4
Statistical analysis results of entrapment efficiency (Y_1), particle size (Y_2), zeta potential (Y_3), burst effect (Y_4) and DE (Y_5).

Parameters	Entrapment efficiency (Y_1)		Particle size (Y_2)		Zeta potential (Y_3)		Burst effect (Y_4)		DE (Y_5)	
	Coefficient	p-value	Coefficient	p-value	Coefficient	p-value	Coefficient	p-value	Coefficient	p-value
Intercept	49.70	<0.0001*	232.66	<0.0001*	−56.12	<0.0001*	22.36	<0.0001*	58.89	0.0002*
X_1(100,300)	23.33	0.0003*	17.14	0.0152*	3.25	0.0046*	3.82	0.0204*	16.29	0.0079*
X_2(300,500)	0.56	0.8425	23.40	0.0043*	−1.87	0.0383*	−0.78	0.5252	−4.24	0.3159
X_3(0.05,0.1)	−16.16	0.0018*	−10.68	0.0737	−1.42	0.0869	−1.96	0.1471	−5.71	0.1940
$X_1 \times X_2$	−0.46	0.9083	−31.47	0.0053*	1.54	0.1638	−0.51	0.7647	−1.5	0.7919
$X_1 \times X_3$	−1.74	0.6648	21.04	0.0255*	0.28	0.7752	1.40	0.4237	−1.14	0.8409
$X_2 \times X_3$	0.12	0.9749	43.90	0.0012*	0.08	0.9319	2.50	0.1823	5.84	0.3269
$X_1 \times X_1$	9.86	0.0539	−14.37	0.0941	−0.42	0.6842	−1.75	0.3440	3.24	0.5873
$X_2 \times X_2$	−0.66	0.8724	2.68	0.7166	−0.56	0.5942	2.52	0.1941	−6.45	0.3014
$X_3 \times X_3$	0.46	0.9103	−0.29	0.9683	0.30	0.7743	0.66	0.7114	−2.17	0.7148

* Most significant value.

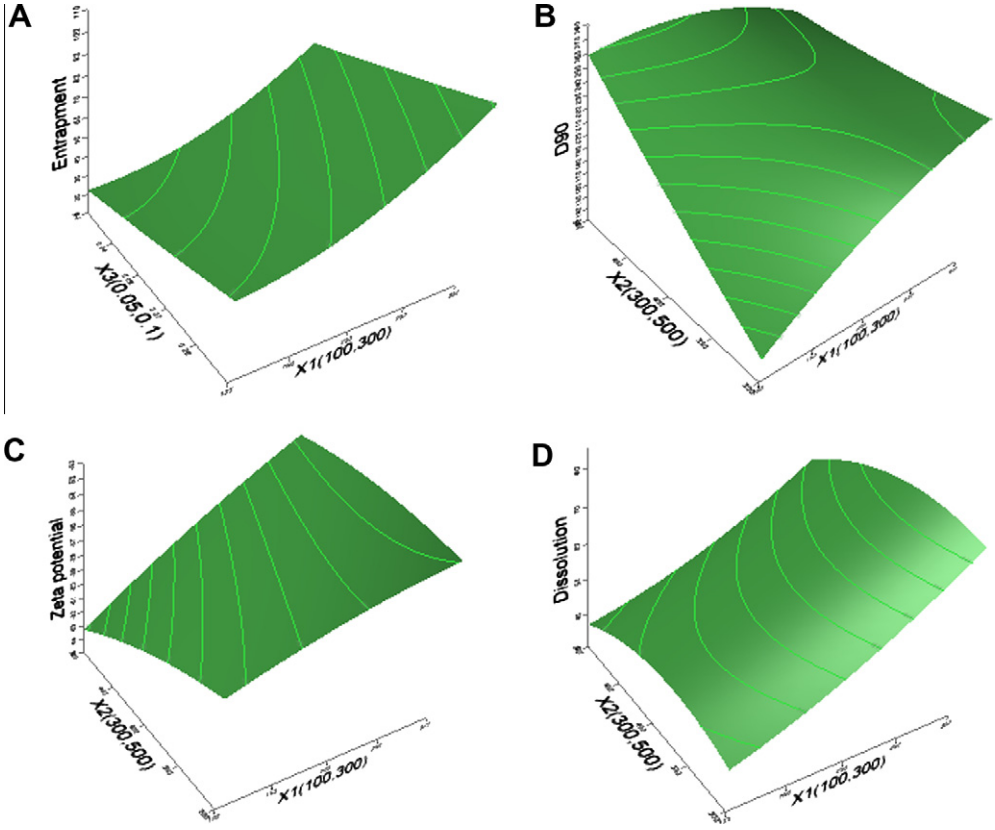

Fig. 1. Surface profilers showing effect of (A) drug (X_1), surfactants (X_3) on entrapment efficiency (Y_1), (B–D) effect of drug (X_1) and lipid (X_3) on D_{90} (Y_2), zeta potential (Y_3) and cumulative percentage release in 8 h (Y_5). (For interpretation of the references to colour in this figure legend, the reader is referred to the web version of this article.)

charge on drug will neutralize the negative charge of lipid and vice versa effect will be observed with increased lipid loading.

3.4. Burst effect (Y_4) and drug release (Y_5)

Drug release from the controlled release formulation often shows the biphasic release pattern and this one was no exception. The first phase was burst release followed by sustained release of risperidone. The reason for the burst release is possibly the drug associated with surface of nanoparticles [28]. Effect of factors on burst release phenomenon could be explained by following equation.

$$Y_4 = 22.36 + 3.82X_1 - 0.78X_2 - 1.96X_3 - 0.51X_1X_2 + 1.40X_1X_3 + 2.50X_2X_3 - 1.75X_1^2 + 2.52X_2^2 + 066X_3^2$$

Similarly, percentage risperidone released in 8 h can be described by following equation

$$Y_5 = 58.89 + 16.29X_1 - 4.24X_2 - 5.71X_3 - 1.50X_1X_2 - 1.14X_1X_3 + 5.84X_2X_3 + 3.24X_1^2 - 6.45X_2^2 - 2.17X_3^2$$

Burst effect (Y_4) and percentage of drug release (Y_5) varied from 15.85 (formulation 5) to 31.41% (formulation 10) and 36.94 (formulation -5) to 77.43% (formulation 10) (Table 3), respectively. Statistical analysis revealed that most significant ($p < 0.05$, Tables 4 and 5 and Fig. 1D) factor affecting the Y_4 and Y_5 was the drug concentration (X_1) employed in the manufacturing of nanoparticles. Interestingly, formulations 5 and 10 represented lowest and highest drug loading formulations and also these formulation employed low and high level of drug in their formulation during manufacture. Further evaluation of data revealed that no interaction and

Table 5
ANOVA results of entrapment efficiency (Y_1), mean particle size (Y_2), zeta potential (Y_3), burst effect (Y_4) and DE (Y_5).

Response	Source	DF	Sum of square	Mean of square	*F* ratio	Prob > *F*[*]
Y_1	Model	9	6828.65	758.74	13.30	0.0054
	Error	5	285.25	57.05		
	Cumulative total	14	7113.90			
Y_2	Model	9	21,901.55	2433.51	13.58	0.0052
	Error	5	895.80	179.16		
	Cumulative total	14	22,797.35			
Y_3	Model	9	140.83	15.65	4.37	0.0594
	Error	5	17.88	3.58		
	Cumulative total	14	158.71			
Y_4	Model	9	224.81	24.98	2.40	0.1741
	Error	5	52.07	10.41		
	Cumulative total	14	276.87			
Y_5	Model	9	2897.01	321.89	2.78	0.1364
	Error	5	579.05	115.81		
	Cumulative total	14	3476.06			

[*] 'Prob > *F*' is the significance level and a value less than 0.05 considered significant.

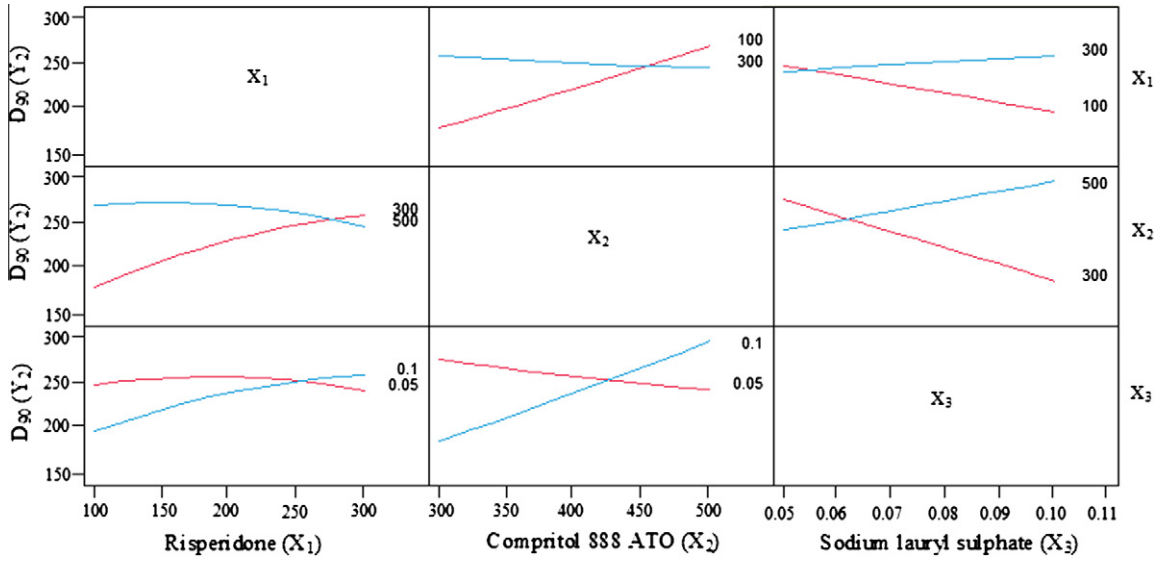

Fig. 2. Interaction profile of drug (X_1), lipid (X_2) and surfactant (X_3) on D_{90} (Y_2). (For interpretation of the references to colour in this figure legend, the reader is referred to the web version of this article.)

quadratic terms have statistically significant ($p > 0.05$) effect on Y_4 and Y_5, respectively.

3.5. Optimization

Desirability function was run using JMP software to get the optimized formulation. The optimum formulation was based on our set criteria of maximum entrapment efficiency, minimum particle size ($D_{90} \leqslant 200$ nm), zeta potential ($\geqslant \pm 30$ mV), minimum burst effect and maximum cumulative percentage release in 8 h. The reason for selecting D_{90} of less than 200 nm is based on the literature report. It is reported by the researcher that particle size greater than 200 nm serves as splenotropic agents and later removed by spleen [10]. Thus, SLN smaller than 200 nm increase its circulation time and hence an increase in the time for which the drug remains in contact with BBB and for the drug to be taken up by the brain [10]. Upon 'trade off' of various responses and comprehensive search through desirability function, the composition of optimized formulation was 200 mg risperidone, 350 mg compritol 888 ATO and 0.1% SLS that fulfill the requirement of optimized formulation. The optimized formulation has entrapment 35 ± 1.23%, D_{90} 175 ± 10.4 nm, zeta potential 58.51 ± 1.23 mV, burst release 17.90 ± 2.02% and cumulative percentage released of risperidone after 8 h 58.83 ± 3.79%, which were in good agreement with the predicted values.

3.6. Physicochemical characterization of nanoparticles

TEM studies revealed that nanoparticles were almost spherical with smooth morphology appeared as black dots (Fig. 3A). FTIR studies were conducted to find out any interaction between risperidone and compritol 888 ATO. FTIR spectrum (Fig. 3B) of risperidone showed absorption bands of C—N stretching between 1000 and 1200 cm^{-1} due to tertiary amine, 2759 and 3000 cm^{-1} C—C stretching due to CH_2 group, 1535 and 3060 cm^{-1} due to C=C stretching of arene ring and 1643 cm^{-1} due to C=O stretching of aromatic ketone. Similarly, compritol 888 ATO revealed absorption bands of C—H stretching at 2815 and 2849 cm^{-1} and C=O stretching at 1738 cm^{-1}. The physical mixture and SLN formulation showed the absorption band corresponding to risperidone and

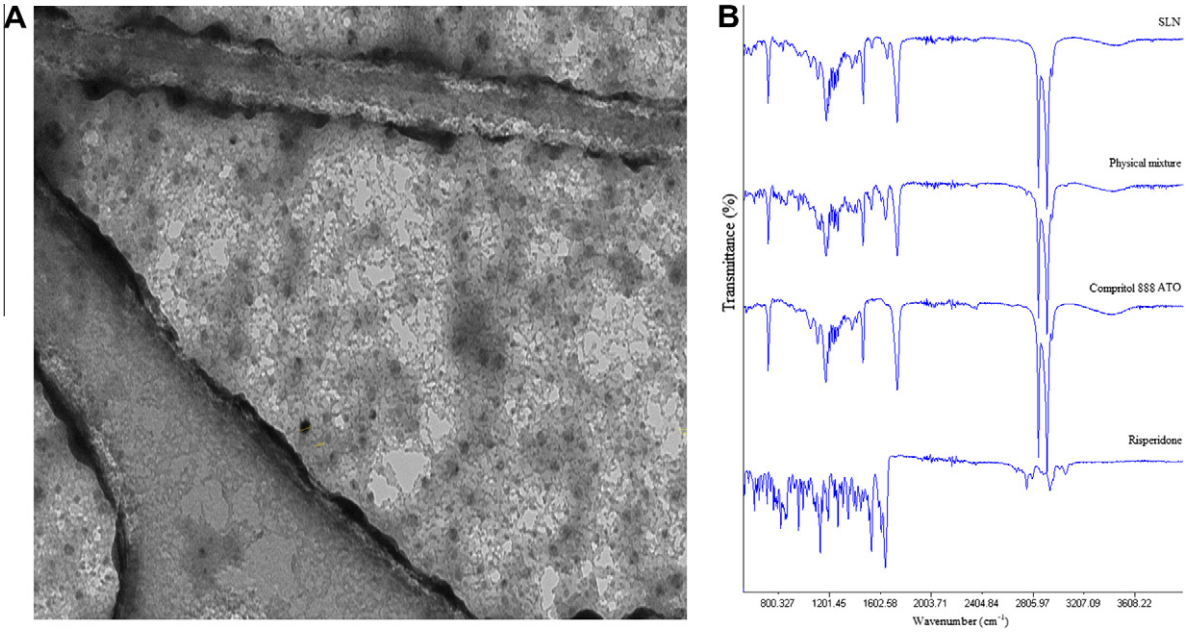

Fig. 3. (A) TEM photomicrographs of solid lipid nanoparticles and (B) FTIR spectrum of risperidone, compritol 888 ATO, their physical mixture and SLN. (For interpretation of the references to colour in this figure legend, the reader is referred to the web version of this article.)

compritol indicating no interaction between these two components of SLN formulation. This was further confirmed by DSC study, which is indicated by appearance of no new peaks or disappearance of peaks. It also points to crystallinity of a compound. Fig. 4A showed the DSC thermogram of risperidone, compritol, their physical mixture and SLN formulation. Risperidone and compritol showed the sharp melting endothermic peaks at 71.2 and 170 °C indicating that starting materials were crystalline. Similarly, their physical mixture showed the peak of both components, while SLN formulation showed characteristics melting peak at 70.8 °C that could be attributed to compritol and showed no peak for the drug indicating the conversion of crystalline risperidone to amorphous form in the SLN formulation or dissolution of risperidone in the melted matrix of compritol 888 ATO. This was further confirmed by X-ray powder diffraction studies (Fig. 4B). Risperidone showed the peaks at 2θ value of 19.7, 20.6, 22.43, 24.58, 27.33, 31.79 and 43.79 and compritol at 20.8 and 22.8° further confirming the crystallinity of both the components. Their physical mixture revealed the peaks of the components, while SLN showed the peak of compritol only indicating that drug lost its crystallinity and it confirmed that risperidone exist in amorphous form in SLN formulations.

3.7. Chemometrics

3.7.1. Near infrared

Very few investigators demonstrated the usefulness of near infrared spectroscopy in estimating the components of novel dosage forms. Researchers showed the application of NIR in estimating cyclosporine and polyethylene glycol from their solid dispersion

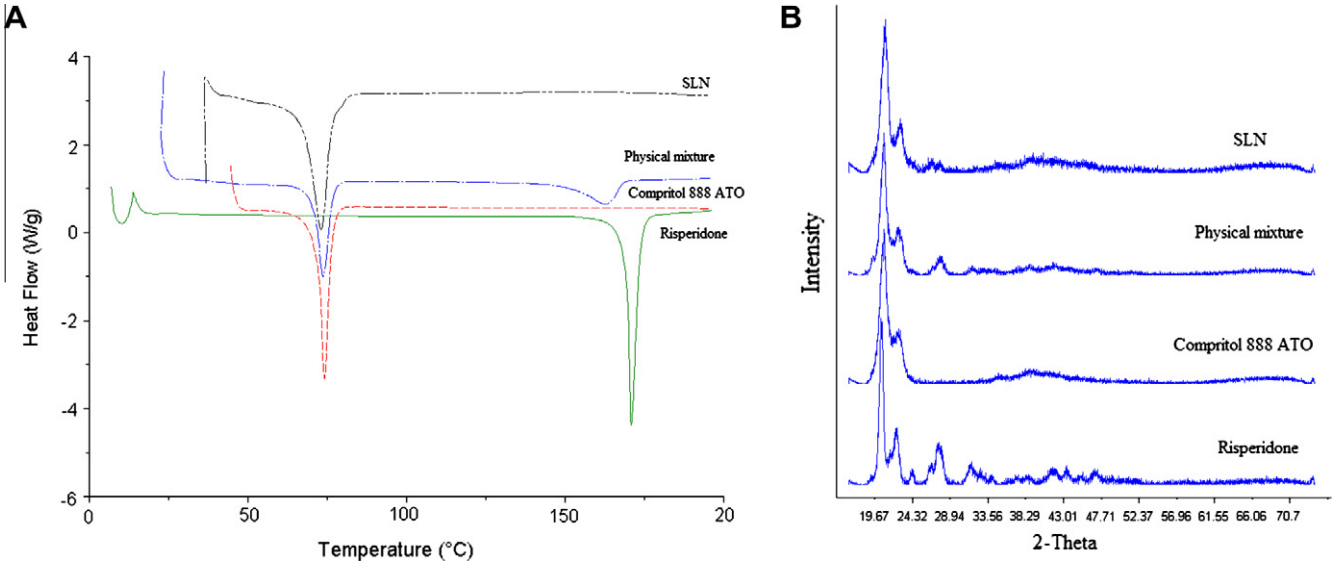

Fig. 4. (A) DSC thermogram and (B) PXRD spectrum of risperidone, compritol 888 ATO, their physical mixture and SLN. (For interpretation of the references to colour in this figure legend, the reader is referred to the web version of this article.)

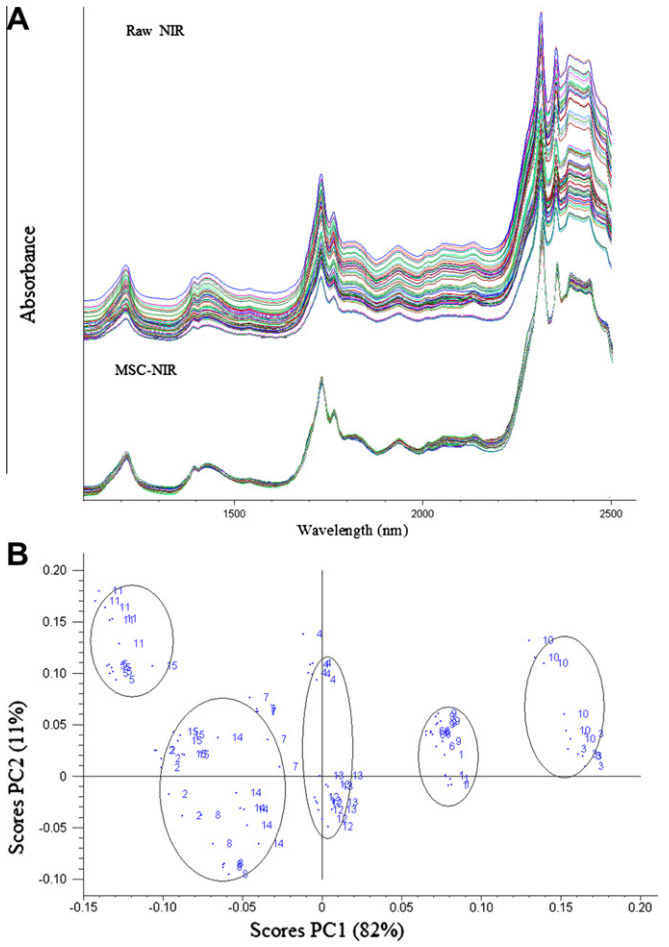

Fig. 5. (A) Raw and multiple scattering corrected NIR spectra of SD formulations and (B) PC1 and PC2 of MSC-NIR spectra of SD formulation computed by principal component analysis. (For interpretation of the references to colour in this figure legend, the reader is referred to the web version of this article.)

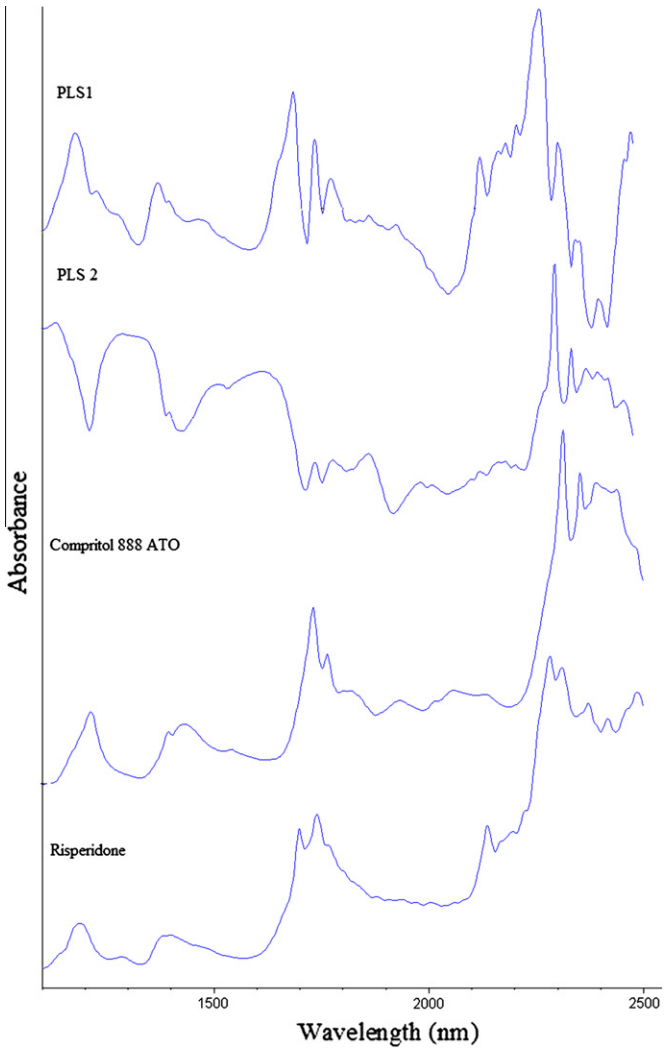

Fig. 6. Loading vectors of the two PLS factors and MSC-NIR spectra of the individual components. (For interpretation of the references to colour in this figure legend, the reader is referred to the web version of this article.)

formulation and cyclosporine from PLGA-based nanoparticles [29,30]. We tried to estimate the components of prepared SLN by NIR. The biggest hurdle in NIR spectroscopy is variation in the collected data. The reason for this variation is multiplicative scattering phenomenon, which arises from different packing density [31] and base line shift [32].

Post-data collection processing methods are reported in the literature to remove these variations such as multiplicative scatter correction (MSC) [33], standard normal variate (SNV) transformation [34], first derivative, second derivative, second derivative/logarithm (SDL) [35]. The parallel shift and base line shift can be removed by derivatives and SDL method but they also add the noise in the data. SNV and MSC are the method of choice for removing multiplicative scattering and also correct for background sloping.

Raw data of SLN formulation were shown in Fig. 5A. Data were treated with first-order, second-order derivatives and SNV method of data correction. None of these method were able to remove these multiplicative and baseline correction except MSC. The data were uniformly divided into calibration and prediction subsets based on the actual drug loading in the SLN formulations. Formulations 1–3, 12–15 were used as calibration set, and formulations 4–11 were used as a prediction set and both these sets represents

Table 6
Results of PLS regression of MSC-NIR data for calibration and prediction of Risperidone and Compritol 888 ATO from SLN formulations.

Parameters	MSC-NIR			
	Risperidone		Compritol 888 ATO	
	Calibration	Prediction	Calibration	Prediction
Number of sample	42	48	42	48
Correlation	0.9969	0.9971	0.9965	0.9971
Offset	0.5024	3.8787	0.1296	1.9809
Slope	0.9938	0.9416	0.9931	0.9417
Root mean square of error	0.9443	1.4007	0.9951	1.4108
Standard error	0.9557	1.1626	1.0072	1.1596

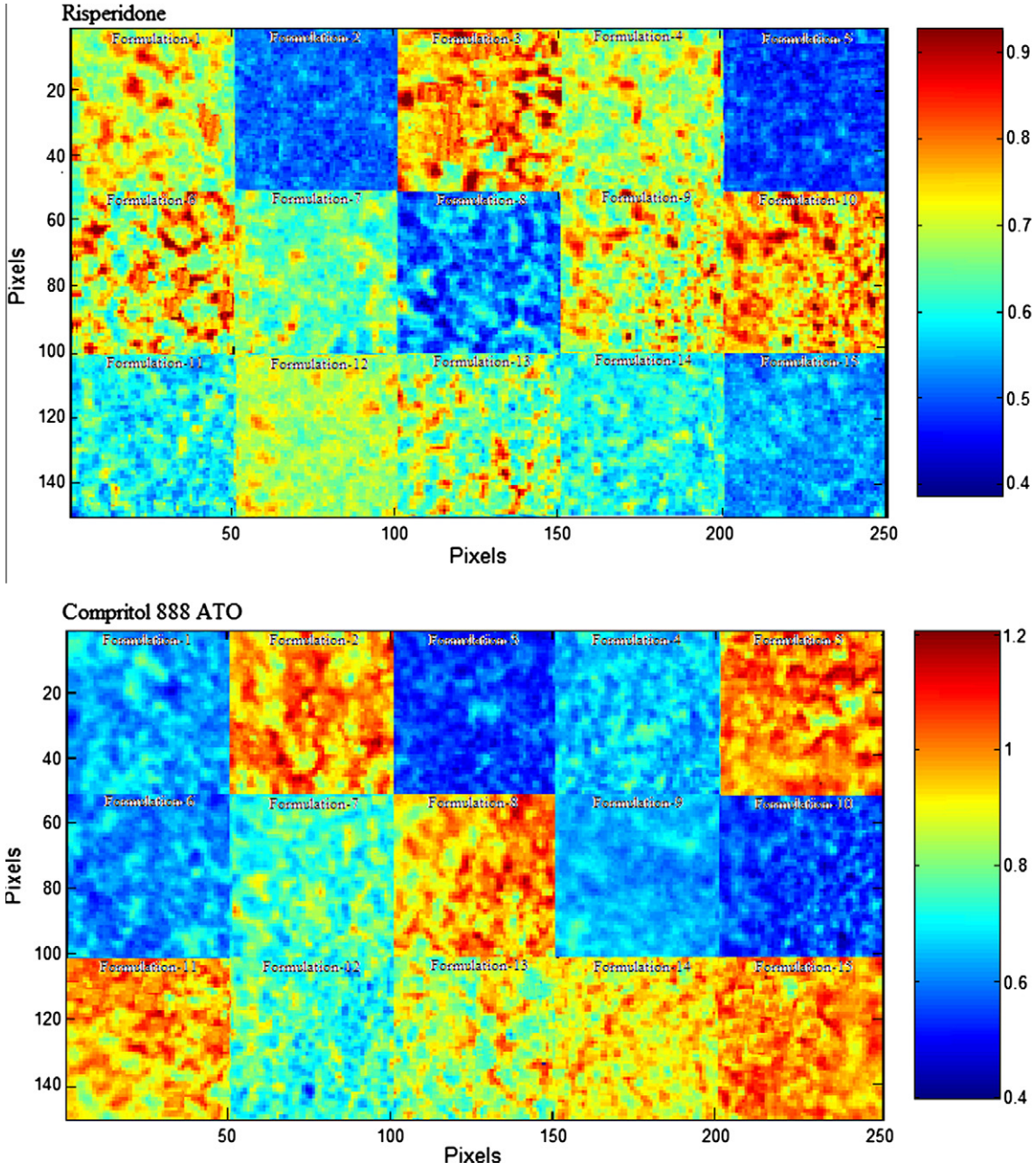

Fig. 7. PLS images showing the distribution of risperidone and compritol 888 ATO in the SLN formulation. (For interpretation of the references to colour in this figure legend, the reader is referred to the web version of this article.)

6.07–40.79% and 5.90–41.67% drug loading in the SLN formulations, respectively. Principal components analysis (PCA) was performed on MSC-NIR data of SLN. Fig. 5B showed the scores of PC1 and PC2 of calibration and prediction data set that represent 82% and 11% variations in the data set, respectively. The PCA analysis allowed successful scattering of 15 formulations and can be grouped into five groups 1, 2 3, 4 and 5 based on their PC1 scores. The approximate value of their PC1 score is −0.13, −0.05, −0.01, 0.08 and 0.17 and can be rank ordered in terms of their PC1 scores, group 1 < group 2 < group 3 < group 4 < group 5 that corresponds to their increasing order of actual drug loading, suggesting that PC1 might represent the risperidone or decreasing loading of compritol 888 ATO.

The most commonly used statistical tools in spectroscopy and chemometrics is the partial least square (PLS) method of multiple regressions mainly because of its less restrictiveness and flexibility over other methods of multiple regressions. PLS method applied to spectroscopic data to build the model for the identification and quantification purpose of components of binary and higher order mixture as well. These objectives are achieved by developing the calibration model and correlation of the instrument responses with the property of interest [36]. The PLS was applied to MSC-NIR data with two PLS factor. PLS1 and PLS2 represent 89% and 9% variation in of MSC-NIR data. Statistics of data of calibration and prediction set was given Table 6 for risperidone and compritol 888 ATO. Correlation coefficient >0.9965 was obtained in all cases indicating the good correlation between calibration and prediction values of risperidone and compritol 888 ATO. The model has good prediction ability as revealed by smaller values of root mean square error of calibration and prediction (RMSEC, RMSEP) and standard error of

Table 7
Results of histogram distributions from PLS score images of SLN formulations.

Formulation	Risperidone			Compritol 888 ATO		
	Number of pixel	Mean ± SD	Skewness	Number of pixel	Mean ± SD	Skewness
1	2480	0.630 ± 0.057	0.256	2481	0.579 ± 0.076	0.319
2	2481	0.389 ± 0.092	0.297	2496	0.865 ± 0.089	0.155
3	2473	0.750 ± 0.076	0.286	2474	0.498 ± 0.061	0.173
4	2489	0.537 ± 0.021	0.220	2483	0.676 ± 0.038	0.180
5	2484	0.387 ± 0.054	0.133	2486	0.881 ± 0.054	0.311
6	2477	0.634 ± 0.032	0.297	2483	0.576 ± 0.022	0.124
7	2472	0.475 ± 0.078	0.317	2485	0.746 ± 0.099	0.301
8	2483	0.395 ± 0.020	0.326	2495	0.856 ± 0.081	0.189
9	2483	0.598 ± 0.087	0.221	2466	0.591 ± 0.007	0.293
10	2476	0.756 ± 0.097	0.269	2482	0.490 ± 0.042	0.232
11	2474	0.437 ± 0.034	0.157	2469	0.825 ± 0.059	0.277
12	2475	0.519 ± 0.086	0.175	2487	0.685 ± 0.063	0.271
13	2464	0.502 ± 0.029	0.274	2471	0.716 ± 0.087	0.258
14	2478	0.443 ± 0.008	0.275	2496	0.815 ± 0.011	0.209
15	2490	0.424 ± 0.033	0.232	2485	0.839 ± 0.096	0.279

calibration and prediction (SEC, SEP), respectively. This indicated that model is equivalent in simultaneously estimating both the components of SLN formulations.

Mean bias and mean accuracy were determined using following equation to assess the accuracy of calibration curve based on the validation data set [37].

$$B_m = \frac{\sum_{i=1}^{n} \frac{(X_c - X_t)}{X_t}}{n} \times 100$$

$$A_m = \frac{\sum_{i=1}^{n} \frac{|X_c - X_t|}{X_t}}{n} \times 100$$

where B_m is the percentage mean bias, Am is the percentage mean accuracy, X_c is the predicted drug/polymer loading value, X_t is actual drug/polymer loading and n is number of experiments. The mean accuracy and bias for risperidone and compritol 888 ATO predictions from MSC-NIR data were 1.60% and 11.27%, and 0.86% and 10.01%, respectively indicating that model is more accurate in predicting risperidone than compritol 888 ATO.

Physical and chemical information contained in the model can be estimated by correlating the PLS factor with chemical and physical property of interest. The PLS factors were compared with the spectra of individual components (Fig. 6). PLS1 showed the positive peaks at 2442, 2408, 2214, 2160, 1768 and 1730 nm and negative peaks at 2492, 2316, 2280, 2222, 2202, 2138, 1792, 1750, 1696, 1382, 1242 and 1192 nm that can be attributed to risperidone. Similarly, PLS2 showed positive peaks and negative peaks at 2316, 2272, 2224, 2140, 1746, 1384, 1224 and 1186 nm, and 1728, 1764, 2158, 2406 and 2438 nm, respectively, which could be due to compritol 888 ATO.

3.7.2. Near infrared chemical imaging

NIR-CI is the non-destructive method of qualitative and quantitative analysis. It provides the spatial distribution of a chemical entity in a substance besides providing the spectral information. Investigators reported its application in the determination of components of complex dosage forms such as nanoparticles [30] and solid dispersion [29]. In this context, we attempted to determine the component of solid lipid nanoparticles by this non-destructive technique. PLS concentration images of SLN formulation were shown in Fig. 7 and concatenated according to risperidone and compritol 888 ATO from prebuilt binary component library containing risperidone and compritol 888 ATO. These images showed the homogenous distribution of risperidone and compritol 888 ATO in the formulation. The histogram (not shown) confirms this symmetry of components of SLN formulation distribution by low value of skew (Table 7). The formulation can be arranged according to intensity of their PLS concentration image representing either risperidone or compritol 888 ATO, and rank order of these PLS concentration images of risperidone in SLN formulation were formulation 5 < formulation 2 < formulation 8 < formulation 15 < formulation 11 < formulation 14 < formulation 7 < formulation 13 < formulation 12 < formulation 4 < formulation 9 < formulation 1 < formulation 6 < formulation 3 < formulation 10 and order will be reversed in case of the compritol. This rank order of PLS concentration image was correlated with the actual loading of risperidone or compritol 888 ATO in the SLN formulations. SLN formulation can be quantized by plotting actual loading of risperidone or compritol and mean representing either risperidone or compritol 888 ATO from their PLS concentration image (Table 7) and revealed R^2 of 0.986 and 0.989 for risperidone and compritol 888 ATO, respectively. Thus, the NIR-CI provided another non-destructive technique for the quantitation of the components of SLN formulations.

4. Conclusions

The novel drug delivery systems of risperidone were prepared and characterized by the state of art technology. The main and interaction effects of selected variables on the critical quality attributes of solid lipid nanoparticles were determined by formal design of experimental strategy. Drug level employed in the manufacture of SLN has statistical influence ($p < 0.05$) over entrapment efficiency, particle size, zeta potential and cumulative percentage released. Entrapment efficiency and D_{90} also was influenced by surfactant and lipid level, respectively. Uniform distribution of risperidone and compritol 888 ATO is revealed by NIR-CI, and good correlation was obtained between actual loadings of risperidone or compritol 888 ATO and mean concentration form PLS image representing either risperidone or compritol. The developed PLS-chemometric model based on the NIR data successfully estimates the components of SLN with good accuracy. This offers the advantage over conventional method of quantitation in that multicomponent of a formulation can be estimated instantaneously and simultaneously after the construction of model.

Acknowledgements

The authors would like to thank the Oak Ridge Institute for Science and Education (ORISE) for supporting post doctoral research program. The views presented in this article do not necessarily reflect the official policy of the US Food and Drug Administration.

References

[1] N.B. Chauhan, Trafficking of intracerebroventricularly injected antisense oligonucleotides in the mouse brain, Antisense Nucl. Acid Drug Dev. 12 (2002) 353–357.
[2] R. Grondin, Z. Zhang, Y. Ai, D.M. Gash, G.A. Gerhardt, Intracranial delivery of proteins and peptides as a therapy for neurodegenerative diseases, Prog. Drug Res. 61 (2003) 101–123.
[3] C. Guerin, A. Olivi, J.D. Weingart, H.C. Lawson, H. Brem, Recent advances in brain tumor therapy: local intracerebral drug delivery by polymers, Invest. New Drugs 22 (2004) 27–37.
[4] A. Misra, S. Ganesh, A. Shahiwala, S.P. Shah, Drug delivery to the central nervous system: a review, J. Pharm. Pharm. Sci. 6 (2003) 252–273.
[5] W.M. Pardridge, Blood–brain barrier drug targeting enables neuroprotection in brain ischemia following delayed intravenous administration of neurotrophins, Adv. Exp. Med. Biol. 513 (2002) 397–430.
[6] M.A. Bagger, E. Bechgaard, The potential of nasal application for delivery to the central brain a microdialysis study of fluorescenin in rats, Eur. J. Pharm. Sci. 21 (2004) 235–242.
[7] M.L. Adams, A. Lavasanifar, G.S. Kwon, Amphiphilic block copolymers for drug delivery, J. Pharm. Sci. 92 (2003) 1343–1355.
[8] R. Saito, J.R. Bringas, T.R. McKnight, M.F. Wendland, C. Mamot, D.C. Drummond, D.B. Kirpotin, J.W. Park, M.S. Berger, K.S. Bankiewicz, Distribution of liposomes into brain and rat brain tumor models by convection-enhanced delivery monitored with magnetic resonance imaging, Cancer Res. 64 (2004) 2572–2579.
[9] H.L. Wong, N. Chattopadhyay, XY Wu, R. Bendayan, Nanotechnology applications for improved delivery of antiretroviral drugs to the brain, Adv. Drug Deliv. Rev. (2009).
[10] I.P. Kaur, R. Bhandari, S. Bhandari, V. Kakkar, Potential of solid lipid nanoparticles in brain targeting, J. Control. Release 127 (2008) 97–109.
[11] C. Freitas, R.H. Müller, Effect of light and temperature on zeta potential and physical stability in solid lipid nanoparticles (SLN) dispersions, Int. J. Pharm. 168 (1998) 221–229.
[12] R.H. Muller, K. Mäder, S. Gohla, Solid lipid nanoparticles (SLN) for controlled drug delivery – a review of the state of the art, Eur. J. Pharm. Biopharm. 50 (2000) 161–177.
[13] S.H. Gohla, A. Dingler, Scaling up feasibility of the production of solid lipid nanoparticles (SLN™), Pharmazie 56 (2001) 61–63.
[14] International conference of harmonization, Pharm. Dev., Q8 (R2), 2009.
[15] G. Box, D. Behnken, Some new three level designs for the study of quantitative variables, Technometrics 2 (1960) 455–475.
[16] S. Chopra, G.V. Patil, S.K. Motwani, Release modulating hydrophilic matrix systems of losartan potassium: optimisation of formulation using statistical experimental design, Eur. J. Pharm. Biopharm. 66 (2007) 73–82.
[17] J.M. Davis, The choice of drugs for schizophrenia, N. Engl. J. Med. 354 (2006) 1846–1848.
[18] J. Yan, Risperidone approved to treat schizophrenia in children, Psychiatric News 42 (2007) 1.
[19] Z. Rahman, K. Kohli, R.K. Khar, M. Ali, N.A. Charoo, A.A.A. Shamsher, Characterization of 5-Fluorouracil microspheres for colonic delivery, AAPS Pharm. Sci. Technol. 7 (2006) E1–E9.
[20] A.P. Suthar, S.A. Dubey, S.R. Patel, A.M. Shah, Determination of Risperidone and forced degradation behavior by HPLC in tablet dosage form, Int. J. Pharm. Technol. Res. 1 (2009) 568–574.
[21] International conference of harmonization–validation of analytical procedures, Q2(R1), 2005.
[22] S. Singh, S.M. Muthu, Preparation and characterization of nanoparticles containing an atyptical antipsychotic agent, Nanomedicine 2 (2007) 233–240.
[23] Z. Rahman, A.S. Zidan, M.J. Habib, M.A. Khan, Understanding the quality of protein loaded PLGA nanoparticles variability by Plackett–Burman design, Int. J. Pharm. (2009).
[24] Y.Y. Yang, T.S. Chung, X.L. Bai, W.K. Chan, Effect of preparation condition on morphology and release profiles of biodegradable polymeric microspheres containing protein fabricated by double-emulsion method, Chem. Eng. Sci. 55 (2000) 2223–2236.
[25] Q. Yang, G. Owusu-Ababio, Biodegradable progesterone microsphere delivery system for osteoporosis therapy, Drug Dev. Ind. Pharm. 26 (2000) 61–70.
[26] P. Couvreur, M.J. Blanco-Prieto, F. Puisieux, B. Roques, E. Fattal, Multiple emulsion technology for the design of microspheres containing peptides and oligopeptides, Adv. Drug Deliv. Rev. 28 (1997) 85–96.
[27] Y.Y. Yang, T.S. Chung, N.P. Ng, Morphology, drug distribution, and in vitro release profiles of biodegradable polymeric microspheres containing protein fabricated by double-emulsion solvent extraction/evaporation method, Biomate 22 (2001) 231–241.
[28] R. Jalil, J.R. Nixon, Microencapsulation using poly(l-lactic acid) I: microcapsule properties affected by the preparation technique, J. Microencapsul. 6 (1989) 473–484.
[29] Z. Rahman, A.S. Zidan, M.J. Habib, M.A. Khan, Formulation and evaluation of a protein loaded solid dispersions by non-destructive methods, AAPS J. (2010).
[30] A.S. Zidan, Z. Rahman, M.J. Habib, M.A. Khan, Spectral and spatial characterization of protein loaded PLGA nanoparticles, J. Pharm. Sci. 99 (2010) 1180–1192.
[31] N. Heigl, C.H. Petter, M. Lieb, G.K. Bonn, C.W. Huck, Near-infrared reflection spectroscopy and partial least squares regression for determining the total carbon coverage of silica packings for liquid chromatography, Vib. Spectrosc. 49 (2009) 155–161.
[32] R.C. Smith, K.S. Baker, Optical properties of clearest natural waters (200–800 nm), Appl. Opt. 20 (1981) 177–184.
[33] P. Geladi, D. MacDougall, H. Martens, Linearization and scatter-correction for near-infrared reflectance spectra of meat, Appl. Spectrosc. 39 (1985) 491–500.
[34] R.J. Barnes, M.S. Dhanoa, S.J. Lister, Standard normal variate transformation and de-trending of near-infrared diffuse reflectance spectra, Appl. Spectrosc. 43 (1989) 772–777.
[35] Y.R. Tahboub, H.L. Pardue, Evaluation of multiwavelength first- and second-derivative spectra for the quantitation of mixtures of polynuclear aromatic hydrocarbons, Anal. Chem. 57 (1985) 38–41.
[36] S.C. Baratieri, J.M. Barbosa, M.P. Freitas, J.A. Martins, Multivariate analysis of nystatin and metronidazole in a semi-solid matrix by means of diffuse reflectance NIR spectroscopy and PLS regression, J. Pharm. Biomed. Anal. 40 (2006) 51–55.
[37] M. Suda, K. Takayama, M. Otsuk, An accurate quantitative analysis of polymorphic content by chemometric X-ray powder diffraction, Anal. Sci. 24 (2008) 451–457.